KSCE Journal of Civil Engineering (2021) 25(5):1746-1754
DOI 10.1007/s12205-021-0670-0

pISSN 1226-7988, eISSN 1976-3808
www.springer.com/12205

Structural Engineering

Experimental Study on the Effect of Boundary Layer on High-Speed Train Aerodynamic Forces Measurement

Zhixiang Huang[a], Weiping Zeng[b], Jie Gai[c], and Hanjie Huang[b]

[a]*State Key Laboratory of Aerodynamics, China Aerodynamics Research and Development Center, Mianyang 621000, China*
[b]*China Aerodynamics Research and Development Center, Mianyang 621000, China*
[c]*Changchun CRRC Railway Vehicles CO., LTD, Changchun 130062, China*

ARTICLE HISTORY

Received 13 April 2020
Accepted 6 December 2020
Published Online 12 February 2021

KEYWORDS

High-speed train
Boundary layer
Aerodynamic coefficients
Reynolds number effect
Wind tunnel test

ABSTRACT

The influences of boundary layer thickness on the aerodynamic characteristics of a high-speed train head car were investigated with an 1:8 scaled model in an 8 m × 6 m wind tunnel at CARDC. Boundary layer thicknesses at different positions on the ballast surface were measured under the wind velocity range of 40 to 70 m/s and the Reynolds number range of 1.25×10^6 to 2.19×10^6. It was found that the effect of Reynolds number on the head car was small. The boundary layer thickness increased significantly along the ballast and decreased gradually with the increase of the wind velocity. A linearly fitted model was employed to calculate the boundary layer thickness under different wind velocities. The changing patterns of the drag and lift force coefficients with the boundary layer thickness were complex. The drag and lift coefficients increased by 5.57% and 21.97% respectively, when the boundary layer thickness was larger than 118 mm. The effects of boundary layer on lift coefficients were more prominent than on the drag coefficients.

1. Introduction

Wind tunnel tests are widely adopted to analyze the aerodynamics characteristics of high-speed trains. Wind tunnel tests have the advantages of high force and pressure measurement accuracy and easy incoming airflow parameter control, and almost not been influenced by the outdoor weather conditions. Wind tunnel tests of trains and vehicles can be classified into two groups: stationary model test (Schober et al., 2010; Sterling et al., 2010; He et al., 2014; Liu et al., 2016) and moving model test (Charuvisit et al., 2004; Li et al., 2013; Yang et al., 2016; Xiang et al., 2017). Stationary model tests are more commonly used to evaluate static aerodynamic characteristics. Dorigatti et al. (2015) reported that the airflow difference between the train model and the full-scale model was as high as 17%; however, this difference could be accepted when the uncertainty of nature wind was considered (Bell et al., 2014). After comparing the boundary layers obtained from model tests and prototype train by the empirical formula, Muld et al. (2013) noticed no significant difference in the flow characteristics of the boundary layers between L_t/H = 12.5, 19, and 25, where H is the model height, including the distance between wheel and surface of the track.

In high-speed train static aerodynamic force measurement tests, large-scale models are generally preferred. Owing to large model lengths and high simulation requirements for ballasts and tracks, boundary layer removing techniques, such as moving belt used in automobile tests are no longer applicable. Huang et al. (2013) simulated the ground effect by a fixed floor. Different from the uniform distribution of the full-scale train, boundary layers at the middle and tail cars of the model were fully developed and much larger than that of the head car. Boundary layers have remarkable influences on the accuracy of force measurements. It should also be noted that the clearance between a high-speed train model bottom and the ballast surface is small, with the combination influence of the boundary layers of the model bottom itself and the ballast surface, the major area of the model bottom becomes submerged in the boundary layer. Consequently, aerodynamic force test results are significantly affected by such a complex state (Sun et al., 2013).

Numerical calculations and experimental works have been conducted to investigate the boundary layer characteristics of full-scale trains (Pereira and André, 2013; Jia et al., 2017; Bell et

CORRESPONDENCE Hanjie Huang hansjie@hotmail.com China Aerodynamics Research and Development Center, Mianyang 621000, China

al., 2020) and model tests (Niu et al., 2016; Zhang et al., 2018). It is generally noticed that the boundary layer thickness increases with the increase of train length. Boundary layer thicknesses on ballast surfaces in wind tunnel tests are usually found to be less than 30% of *H*, thereby satisfying the requirements of the European Standard (2008, 2009 and 2010). However, for large-scale train model tests, very few works on the influence of wind velocity on boundary layer distributions and the quantitative influences of boundary layer thickness on aerodynamic forces, especially key parameters of drag and lift force coefficients are available. Hence, effective and adaptive force correction methods based on wind tunnel tests are still lacking for practical high-speed train aerodynamic design.

In the pesent experimental research, the aerodynamic characteristics of a high-speed train head car were investigated with an 1:8 scaled model at different locations on the ballast and track in fixed floor. The main focuses of this work were to analyze the boundary layer characteristics on the ballast, the influences of wind velocity on the boundary layer thickness, and the influences of the boundary layer on aerodynamic forces. A credible scientific basis is tried to provide for the further development of correction methods for the ground effect.

2. Overview of the Experiment

2.1 Test Facility

Wind tunnel tests were conducted in the second test section of a 12 m × 16 m /8 m × 6 m low speed wind tunnel at the China Aerodynamics Research and Development Center (CARDC) (Fig. 1). The length of the second test section is 15 m and its cross-sectional area is 47.4 m^2. The minimum and maximum wind speeds are 20 m/s and 80 m/s, respectively.

The wind tunnel was equipped with a special train test platform (length = 15.16 m) consisting of several flat plates. This test platform was used as the fixed floor for ground effect simulations. As shown in Fig. 2, the flat plates were supported by a bracket to enhance structural stability and reduce the blocking ratio. A turntable of 7 m diameter was placed on the test platform for wind angle tests.

The height between the platform surface and the test section floor was 1.06 m.When the test platform was installed in the wind tunnel test section, the effective length, width, height, cross-sectional area of the test section were 15.16 m, 8 m, 4.94 m, and 39.2 m^2, respectively. The distance from the turntable center to the test platform's leading edge was 7.84 m. To reduce flow disturbance, test platform's leading and trailing edges were made streamline-shaped. Flow-disturbance slices were fixed at the back edge of each plate; thus low-pressure regions of the vortex were generated in the gaps between two adjacent plates to suck the low-energy flow on the surface of platform, and make the boundary layer thickness decrease. The parameters of flow quality are presented in Table 1.

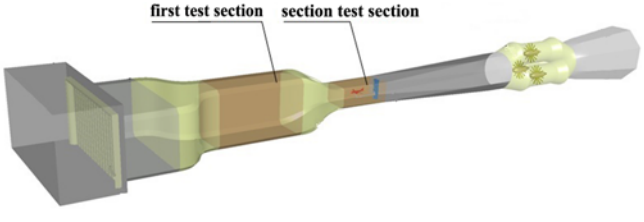

Fig. 1. Schematic of the 8 m × 6 m Wind Tunnel

(a)

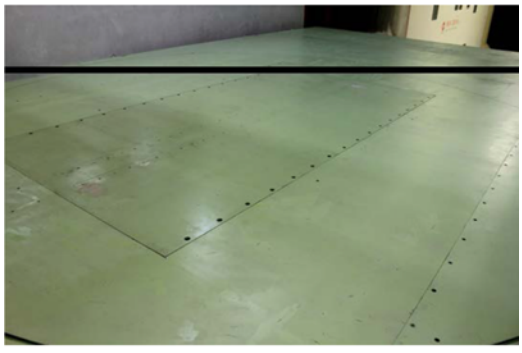

(b)

Fig. 2. Train Test Platform: (a) Bracket, (b) Flat Plates

Table 1. Parameters of Flow Quality

Items	Index
Flow stability	0.005
Dynamic pressure coeffcient	≤ 0.5%
Direction field	$\alpha_i \leq 0.5°$, $\beta_i \leq 0.5°$
Turbulence intensity	≤ 0.2%
Axial static pressure coeffcient	-0.0003 (empty), -0.002 (test platform)

A 14.5 m long ballast model was installed on the platform, and a track model was located on the ballast surface. Specific slopes were used for the two ends of the ballast as the platform's leading and trailing edges. A head car train model of China Railway High-speed (CRH) with a scale ratio of 1:8 was mounted on the ballast (Fig. 3). The length, height, width, and cross-sectional area of the head car model were 3.49 m, 0.47 m, 0.42 m, and 0.1856 m^2, respectively. The outside body of the train model was shaped by synthetic resin plates, and its inside structure was built with a metal frame.

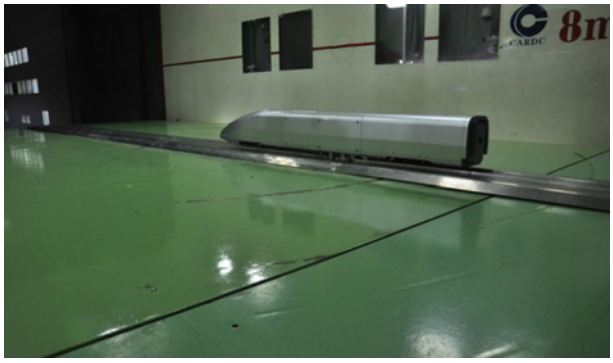

Fig. 3. Test Model of the High-Speed Train Head Car on the Ballast

A force balance unit was welded on the inside frame of the model by a joint plate and it was welded with the ballast by four supporting struts. These supporting struts crossed through the bottom plate of the model, and a 3 mm orbicular gap was kept between each strut and the bottom plate to avoid collisions between them (Fig. 4).

An arc-shaped part was cut off from the lower edge of each bogie wheel, and a 5 mm gap between each bogie wheel and the track was kept to make the train body a separate force-measuring unit (Xiao et al., 2013).

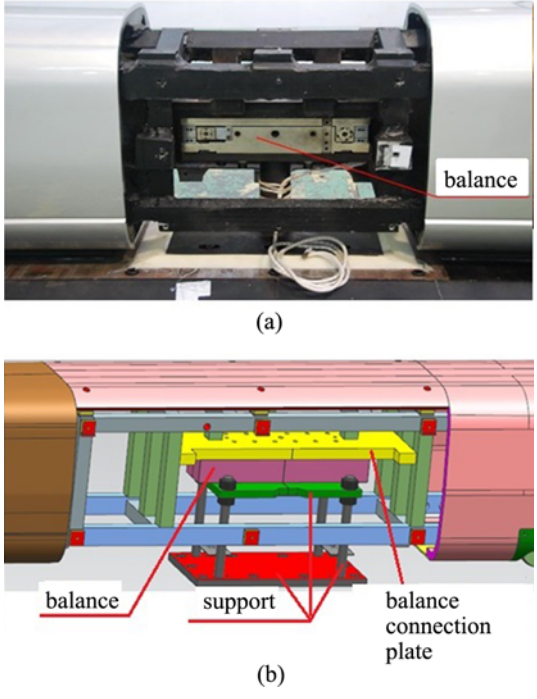

Fig. 4. Sketch Map of Balance and Support: (a) Box-Type Balance, (b) Support Installation

The maximum boundary layer thickness on the ballast with implications for force measurement test was less than 0.325*H* (153 mm), which satisfied the requirement of the European Standard (2008, 2009, and 2010). Above the boundary layer, turbulence intensity of the airflow was approximate no more than 0.2%.

2.2 Measurement Setup

Boundary layer thicknesses on the ballast surface were measured by a pressure rake (height = 400 mm) consisting of 40 probes. These probes were connected to a high-frequency pressure-scanning valve (ZOC33/64Px) with a measuring range 5,000 Pa and an accuracy of 0.08% FS.

The pressure rake could be moved to designated place by a rack mounted on the ballast. The pressure rake was located at the track center, and the probes were perpendicular to the incoming flow. With no train model, boundary layer thicknesses were measured at seven selected monitoring points along the center-line of the ballast surface (Fig. 5). The distances of these points to the front edge of the ballast were 2,200 mm, 4,150 mm, 6,170 mm, 7,220 mm, 9,355 mm, 10,615 mm and 12,255 mm. The probes used for total pressure and static pressure measurement were parallel to the direction of the incoming flow. Each probe was connected to an electric scan valve channel through a soft pipe.

A six-component box-type force balance unit (TH1004B) was used to detect the aerodynamic force in this experiment. The performance parameters of TH1004B are listed in Table 2. The fixed connection between the head car model and the force balance unit guaranteed the accurate transfer of loads. A PXI system with 128 asynchronous channels and an 18-bit A/D digitizer was used for data acquisition. The data sampling frequency was 500 Hz, and the sampling time was no less than 20 s.

During aerodynamic force measurements, six reference positions being the projection point of the head car model's nose-tip, were selected along the center-line of the ballast surface, and the distances of these six positions to the front edge of the ballast

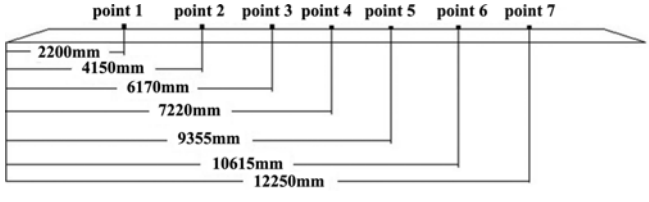

Fig. 5. Measuring Points for Boundary Layer Measurements

Table 2. Parameters of the TH1004B Force Balance Unit

Balance unit TH1004B	Lift force	Drag force	Pitching moment	Lateral force	Yaw moment	Overthrow moment
Design Load (*N*, *N·m*)	3,000	300	1,000	2500	1000	300
Precision (%)	0.03	0.03	0.05	0.05	0.03	0.05
Accuracy (%)	0.05	0.05	0.05	0.05	0.10	0.30

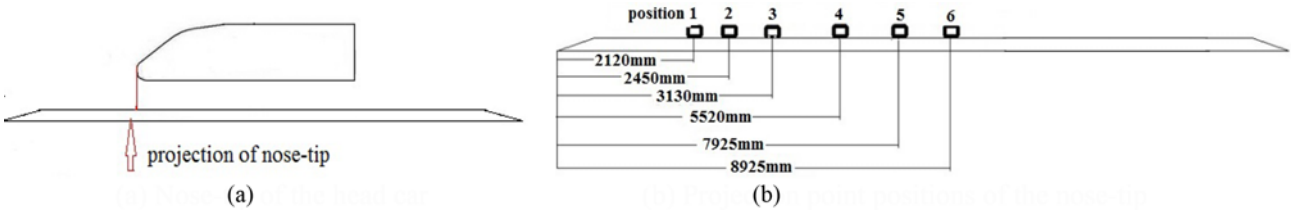

Fig. 6. Positions of the Head Car Model during Aerodynamic Force Measurements: (a) Nose-Tip of the Head Car, (b) Projection Point Positions of the Nose-Tip

were 2,120 mm, 2,450 mm, 3,130 mm, 5,520 mm, 7,925 mm, and 8,925 mm (Fig. 6). It is worth mentioning that because of the limitation of the test platform length, force measurement tests were conducted only for the head car.

2.3 Aerodynamic Coefficients

Aerodynamic force measurement tests were conducted with a yaw angle of 0°. Aerodynamic forces (drag and lift) were normalized non-dimensionally.

$$C_x = \frac{F_x}{\frac{1}{2}\rho V_{ref}^2 S}, \tag{1}$$

$$C_y = \frac{F_y}{\frac{1}{2}\rho V_{ref}^2 S}, \tag{2}$$

where F_x and F_y are the head car model's drag and lift force in body axis system, C_x and C_y are the drag and lift force coefficients, S is the reference area of the model (0.1856 m^2), V_{ref} is the mean speed of the incoming flow, and ρ is the air density at local site (1.2 kg/m^3).

3. Results and Discussion

3.1 Boundary Layer Measurement

To illuminate the distribution of the stream-wise flow velocity profile, boundary layers at different positions along the ballast on the special test platform were measured under the mean incoming flow velocity range of 40 m/s to 70 m/s and the corresponding Reynolds number range of 1.25×10^6 to 2.19×10^6.

The mean velocity profiles at seven different positions on the ballast without a train model under different wind velocities are displayed in Fig. 7. The boundary layer thicknesses along the flow direction, which are the wall-normal coordinates for the stream-wise velocity of $0.99V_{ref}$, are presented in Table 3.

It is noticeable that the detected profiles had almost the same shape under different incoming airflow velocities; however, the lower shape of the wind velocity profiles in the boundary layer became more close to the exponential curve with the increasing distance under the same velocity, thereby the gradients of the velocity profiles also became larger.

It is evident from Table 3 that the boundary layer thickness at each point from $1^{\#}$ to $7^{\#}$ decreased gradually with the increase of the wind velocity. Therefore, the maximum and minimum thicknesses were obtained under the velocities of 40 m/s and 70 m/s. The thickness difference at each point from $1^{\#}$ to $7^{\#}$ was small and the values were 1.4 mm and 11.2 mm at point $1^{\#}$ and $7^{\#}$. Under the same wind velocity, the boundary layer thickness increased more prominently from the forward to rearward along the ballast surface, and the increments in all cases were all larger than 130 mm.

The relationship between boundary layer thicknesses and measuring point distances to the front edge of the ballast appeared to be linear (Fig. 8). The distribution patterns of the boundary layer thickness under different velocities were found to be the same. A linearly fitted model for boundary layer thicknesses with measuring point distances under different velocities is also provided in Fig. 8,

$$\delta = 0.0146X - 1.8952, \tag{3}$$

where δ is the boundary layer thickness (mm) and X is the distance of each measuring point to the front edge of the ballast (mm).

Under the large wind velocity range, Eq. (3) was quite suitable to

Table 3. Boundary Layer Thicknesses at Different Measuring Points

	40 m/s	45 m/s	50 m/s	55 m/s	60 m/s	65 m/s	70 m/s
Point 1	34.3 mm	34.3 mm	34.2 mm	33.9 mm	33.5 mm	33.4 mm	32.9 mm
Point 2	59.4 mm	59.2 mm	59.0 mm	58.9 mm	58.5 mm	58.2 mm	57.8 mm
Point 3	84.8 mm	84.5 mm	84.1 mm	83.1 mm	82.8 mm	82.2 mm	82.0 mm
Point 4	110.9 mm	108.9 mm	103.7 mm	98.8 mm	98.3 mm	97.9 mm	97.6 mm
Point 5	150.8 mm	149.6 mm	148.4 mm	148.3 mm	148.0 mm	147.8 mm	147.2 mm
Point 6	165.8 mm	165.5 mm	163.1 mm	161.4 mm	161.1 mm	161.0 mm	160.6 mm
Point 7	178.7 mm	174.4 mm	171.5 mm	171.4 mm	170.7 mm	168.9 mm	167.5 mm

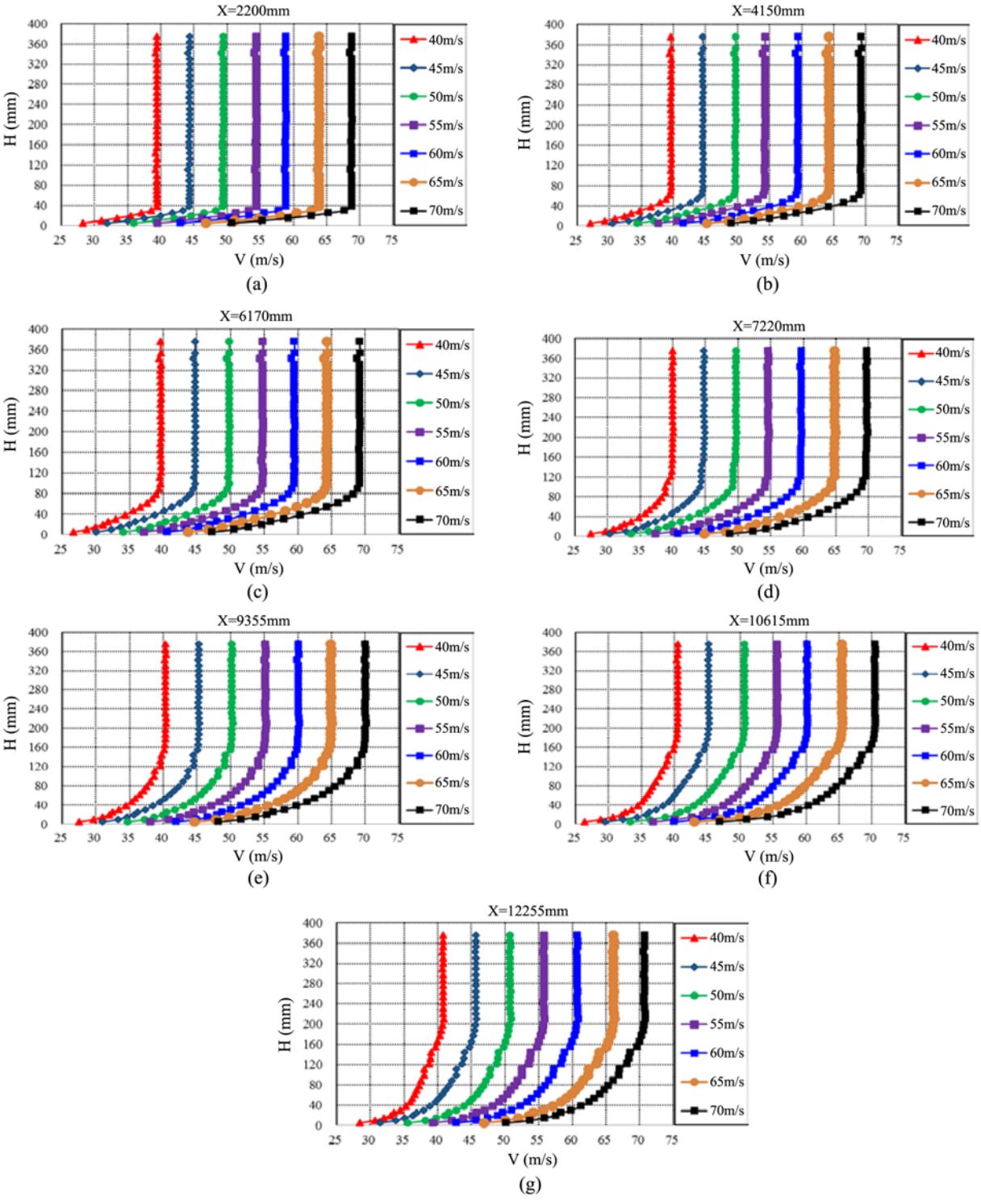

Fig. 7. Stream-Wise Flow Velocity Profiles at Different Position (1# to 7#) along the Ballast under the Mean Incoming Flow Velocity Range of 40 m/s to 70 m/s: (a) x = 2,200 mm, (b) x = 4,150 mm, (c) x = 6,170 mm, (d) x = 72,200 mm, (e) x = 9,355 mm, (f) x = 10,615 mm, (g) x = 12,255 mm

determine the boundary layer thickness at each measuring point. Boundary layer thicknesses at the projection points of head car nose-tip along the ballast were computed by linear interpolation, and the obtained results with the maximum value of 142.8 mm are presented in Table 4.

3.2 Effect of Reynolds Number

Niu et al. (2016) reported that the influences of Reynolds number on the aerodynamic characteristic of a streamlined, head-shape CRH high-speed train was significant. Reynolds number greatly affected the boundary layer thickness on the train surface,

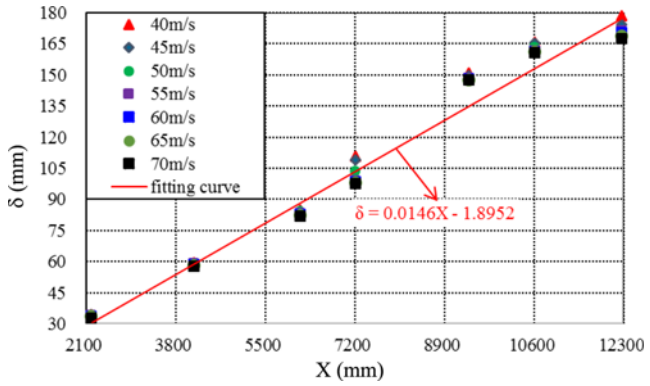

Fig. 8. Distribution Patterns of the Boundary Layer Thickness

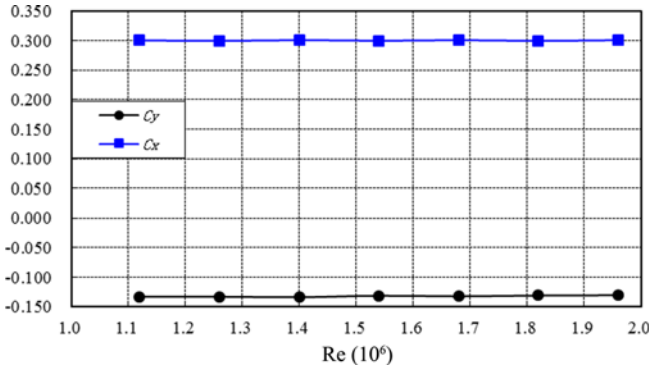

Fig. 9. Changes of the Force Coefficients with Reynolds Number

resulting in changes in the surface pressure distribution and the aerodynamic load. Huang et al. (2013) asserted that change of the wind velocity conformed to the independence principle of Reynolds number for high-speed train force measurement test. When the Reynolds number reached 1.0×10^6, the aerodynamic coefficient changed insignificantly with the increase of Reynolds number. According to the European Standard (2009) and Bell et al. (2014), high-speed train model tests should be conducted at a critical Reynolds number greater than 2.5×10^5 or 1.0×10^6, and the latter value is more generally accepted. When the Reynolds number is larger than 1.0×10^6, it is often noticed that flow structures do not change significantly. The Reynolds numbers calculated with the height of the test model were all larger than 1.0×10^6.

The incoming average wind speeds in the present experiment were 40 m/s, 45 m/s, 50 m/s, 55 m/s, 60 m/s, 65 m/s and 70 m/s, the corresponding Reynolds numbers were 1.25×10^6, 1.41×10^6, 1.57×10^6, 1.72×10^6, 1.88×10^6, 2.04×10^6 and 2.19×10^6, respectively. Reynolds number was calculated by Eq. (4),

$$Re = \frac{\rho V_{ref} H}{\mu}, \tag{4}$$

where $H = 0.47$ m, it is the height of the head car model; $\mu = 1.8 \times 10^{-5}$ Pa.s, is the air viscosity coefficient.

The drag and lift coefficients of the head car at position 1 (distance to the front edge of the ballast = 2,120 mm) were analyzed at the wind angle of 0° under different velocities. It is clear from Fig. 9 and Table 5 that as the wind velocity increased from 40 m/s to 70 m/s, the changes of the coefficients were smaller. It inferred that the errors of the drag and lift coefficients were only 0.2% and 1.92%, respectively, and the aerodynamic force coefficients changed very little when the velocity was larger than 50 m/s. Similar changes of the force coefficients were also noticed at other positions. It can be concluded that when the wind velocity was larger than 60 m/s, its influence on the force coefficients of the head car was small.

3.3 Effect of Boundary Layer Thickness on Aerodynamic Characteristics

Aerodynamic forces on the one head car model of high-speed train were measured at six positions along the ballast. The drag and lift force coefficients were found to change significantly with the increasing boundary layer thickness at the head car nose-tip (Fig. 10).

It is clear that the changing patterns of C_x and C_y under different incoming airflow velocities were almost the same. In comparison to wind velocity, the boundary layer thickness manifested greater impacts on the force coefficients.

Table 4. Boundary Layer Thicknesses at Different Projection Points of the Head Car Nose-Tip

	40 m/s	45 m/s	50 m/s	55 m/s	60 m/s	65 m/s	70 m/s
Position 1	33.4 mm	33.3 mm	33.2 mm	32.9 mm	32.5 mm	32.4 mm	31.9 mm
Position 2	37.6 mm	37.5 mm	37.4 mm	37.1 mm	36.7 mm	36.6 mm	36.1 mm
Position 3	46.3 mm	46.2 mm	46.0 mm	45.8 mm	45.4 mm	45.2 mm	44.8 mm
Position 4	76.6 mm	76.4 mm	76.0 mm	75.3 mm	75.0 mm	74.5 mm	74.2 mm
Position 5	124.1 mm	122.3 mm	118.5 mm	115.1 mm	114.7 mm	114.4 mm	114.1 mm
Position 6	142.8 mm	141.4 mm	139.4 mm	138.3 mm	138.0 mm	137.7 mm	137.6 mm

Table 5. Force Coefficients of the Head Car at Position 1 (C_x = drag coefficient and C_y = lift coefficient)

	40 m/s	45 m/s	50 m/s	55 m/s	60 m/s	65 m/s	70 m/s	Error range
C_x	0.295	0.293	0.294	0.293	0.293	0.293	0.293	0.24%
C_y	-0.127	-0.125	-0.124	-0.122	-0.121	-0.121	-0.120	1.92%

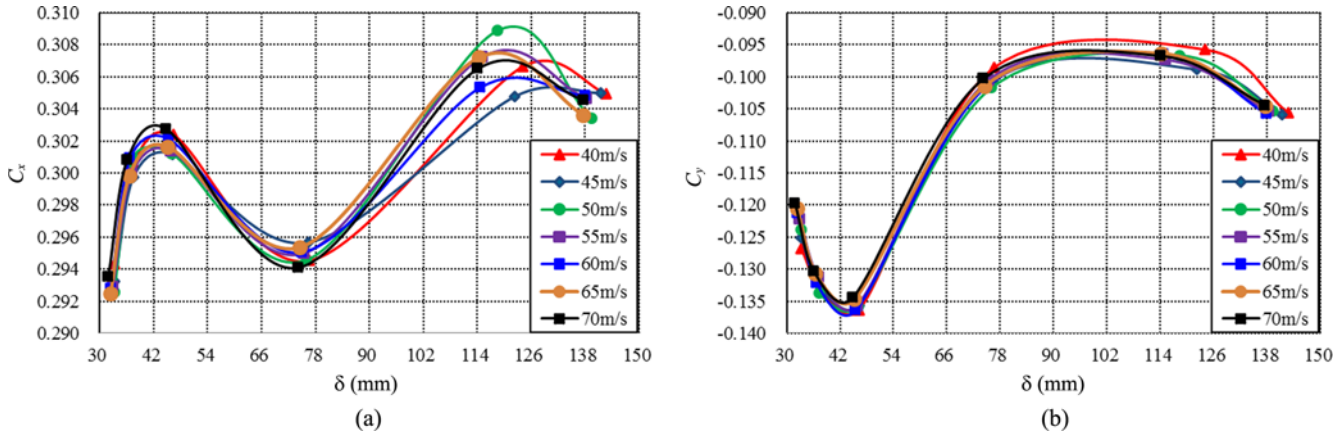

Fig. 10. C_x and C_y Values of the Head Car under Different Boundary Layer Thicknesses: (a) C_x, (b) C_y

The changing patterns of C_x and C_y with the boundary layer thickness seemed to be rather complicated. The value of C_x increased and decreased alternately with the boundary layer thickness changing. Under all test velocities, the maximum values of C_x were found at position 5. The value of C_y first decreased with the increase of the boundary layer thickness, then increased steadily to the point beyond position 5, and finally, decreased at position 6. Under all test velocities, the maximum absolute values of C_y were detected at position 2.

The aerodynamic force coefficients at position 1 were selected as the standard value. The force coefficients at the other positions were compared with those of position 1, and the percentage differences of C_x and C_y are presented in Tables 6 and 7, respectively. Under the incoming airflow velocities range of 40 to 70 m/s, at the other positions (from position 2 to position 6), the percentage differences range of C_x were 0.07% to 4.18%, 0.82% to 3.99%, 0.68% to 5.57%, 0.72% to 4.88%, 0.79% to 4.27%, 0.99% to 5.03% and 0.20% to 4.43%, respectively. It is clear that the percentage differences of C_x at positions 2, 3, 4 were smaller than those at position 5 and 6. Similarly, the percentage difference of C_y at the other positions were -4.89% to 24.53%, -6.16% to 20.94%, -8.00% to 21.97%, -7.36% to -20.38%, -8.99% to 20.53%, -8.46% to 20.07% and -8.76% to 19.28%, respectively. Therefore, the percentage differences of C_y at positions 4, 5, and 6 were larger than those at positions 2 and 3.

It can be inferred that the effects of boundary layer thickness on the aerodynamic characteristics were obvious. The effect of Reynolds number was very small under velocity larger than 50 m/s. The drag and lift coefficients increased by 5.57% and 21.97% under velocity of 50 m/s, when the head car was located at position 5 (boundary layer thickness = 118.5 mm). The influence of boundary layer on C_y was more prominent than on C_x.

According to the European Standard (2008, 2009, 2010), the boundary layer thickness in wind tunnel tests should be less than 30% of the train model height. In this experiment, the height of the 1:8 scaled head car model was 0.47 m. The boundary layer

Table 6. Percentage Differences of C_x at Different Positions

	40 m/s	45 m/s	50 m/s	55 m/s	60 m/s	65 m/s	70 m/s
Position 1	--	--	--	--	--	--	--
Position 2	2.14%	2.22%	2.87%	2.42%	2.77%	2.50%	2.49%
Position 3	2.75%	2.69%	2.94%	2.90%	3.18%	3.11%	3.17%
Position 4	0.07%	0.82%	0.68%	0.72%	0.79%	0.99%	0.20%
Position 5	4.18%	3.92%	5.57%	4.88%	4.27%	5.03%	4.43%
Position 6	3.60%	3.99%	3.69%	4.03%	4.10%	3.79%	3.78%

Table 7. Percentage Differences of C_y at Different Positions

	40 m/s	45 m/s	50 m/s	55 m/s	60 m/s	65 m/s	70 m/s
Position 1	--	--	--	--	--	--	--
Position 2	-4.89%	-6.16%	-8.00%	-7.36%	-8.99%	-8.46%	-8.76%
Position 3	-7.57%	-8.39%	-9.69%	-11.05%	-12.53%	-11.69%	-12.27%
Position 4	22.24%	19.58%	17.85%	17.76%	16.32%	15.92%	16.28%
Position 5	24.53%	20.94%	21.97%	20.38%	20.53%	20.07%	19.28%
Position 6	16.72%	15.43%	14.94%	13.83%	12.78%	13.27%	12.85%

thicknesses at position 2 to 6 were smaller than 30% of the scaled model height (0.47 m). Although compared with the prominent effect by the boundary layer on thickness C_y, C_x are less affected, it should also be noted that bias up to 5.57% changing in C_x is not a small value for practice use in aerodynamic design for high-speed train. These experimental data could be useful for improving the correction method for the ground effect problem.

4. Conclusions

Wind tunnel tests were conducted to study the aerodynamic characteristics of high-speed train head car at different positions on the ballast surface under a wide range of Reynolds number. The effect of Reynolds number was found to be small. The main purpose of this analysis was to study the influences of the boundary layer thickness on the aerodynamic force coefficients of 1:8 scaled head car model. The main observations are presented below.

1. The boundary layer thickness increased significantly from forward to rearward on the ballast surface under the same wind velocity and decreased gradually with the increasing velocity. The influence of wind velocity on the boundary layer thickness was small. A linearly fitted model was used to calculate boundary layer thicknesses at different positions under different velocities.
2. The aerodynamic coefficients of drag and lift changed insignificantly under velocity larger than 50 m/s. Considering the Reynolds number effect on aerodynamic coefficients, the wind velocity of 60 m/s was selected as the optimal value for the 1:8 scaled high-speed train model tests.
3. The drag and lift force coefficients were affected by the boundary layer. The changing patterns of C_x and C_y of the head car were complex. The value of C_x and C_y increased to 5.57% and 21.97% when the boundary layer thickness is 118.5 mm, which is still less than 30% of model height. The effects of boundary layer thickness on C_y were more prominent than on C_x.
4. This research reveals that the ground effect should be considered when the test data are applied to the aerodynamic design of real vehicles; therefore, further developments of the ground simulation technology and the ground effect correction method are required.

Acknowledgments

This work was financially supported by the National Natural Science Foundation of China (Grant No. 51778381 and Grant No. 52078437). We thank LetPub (www.letpub.com) for its linguistic assistance.

ORCID

Hanjie Huang https://orcid.org/0000-0003-1155-9742

References

Bell JR, Burton D, Thompson MC (2020) The boundary-layer characteristics and unsteady flow topology of full-scale operational inter-modal freight trains. *Journal of Wind Engineering & Industrial Aerodynamics* 201:104164, DOI: 10.1016/j.jweia.2020.104164

Bell JR, Burton D, Thompson MC, Herbst AH, Sheridan J (2014) Wind tunnel analysis of the slipstream and wake of a high-speed train. *Journal of Wind Engineering & Industrial Aerodynamics* 134:122-138, DOI: 10.1016/j.jweia.2014.09.004

CEN European Standard (2008) EN 14067-6:2008, Railway applications aerodynamics Part 6: Requirements and test procedures for crosswind assessment. CEN-CENELEC Management Centre, Brussels, Belgium

CEN European Standard (2009) EN 14067-6:2009, Railway applications-aerodynamics Part 6: Requirements and test procedures for crosswind assessment. CEN-CENELEC Management Centre, Brussels, Belgium

CEN European Standard (2010) EN 14067-6:2010, Railway applications-aerodynamics Part 6: Rquirements and test procedures for cross wind assessment. CEN-CENELEC Management Centre, Brussels, Belgium

Charuvisit S, Kimura K, Fujino Y (2004) Effects of wind barrier on a vehicle passing in the wake of a bridge tower in cross wind and its response. *Journal of Wind Engineering & Industrial Aerodynamics* 92(7-8):609-639, DOI: 10.1016/j.jweia.2004.03.006

Dorigatti F, Sterling M, Baker CJ, Quinn AD (2015) Crosswind effects on the stability of a model passenger train - A comparison of static and moving experiments. *Journal of Wind Engineering & Industrial Aerodynamics* 138:36-51, DOI: 10.1016/j.jweia.2014.11.009

He X, Zou Y, Wang H, Han Y, Shi K (2014) Aerodynamic characteristics of a trailing rail vehicles on viaduct based on still wind tunnel experiments. *Journal of Wind Engineering & Industrial Aerodynamics* 135:22-33, DOI: 10.1016/j.jweia.2014.10.004

Huang ZX, Chen L, Zhang WZ (2013) Study on simulation manner of wind tunnel test of high-speed train model. *Journal of Railway Science and Engineering* 10(3):87-93, DOI: 10.19713/j.cnki.43-1423/u.2013.03.018 (in Chinese)

Jia LR, Zhou D, Niu JQ (2017) Numerical calculation of boundary layers and wake characteristics of high-speed trains with different lengths. *PLoS ONE* 12(12):e0189798, DOI: 10.1371/journal.pone.0189798

Li Y, Hu P, Cai CS, Zhang M, Qiang S (2013) Wind tunnel study of a sudden change of train wind loads due to the wind shielding effects of bridge towers and passing trains. *Journal of Engineering Mechanics* 139(9):1249-1259, DOI: 10.1061/(asce)em.1943-7889.0000559

Liu X, Han Y, Cai CS, Levitan M, Nikitopoulos D (2016) Wind tunnel tests for mean wind loads on road vehicles. *Journal of Wind Engineering & Industrial Aerodynamics* 150:15-21, DOI: 10.1016/j.jweia.2015.12.004

Muld T, Efraimsson G, Hennigson DS (2013) Wake characteristics of high-speed trains with different lengths. *Journal of Rail Rapid Transit* 228(4):333-342, DOI: 10.1177/0954409712473922

Niu JQ, Liang XF, Zhou D (2016) Experimental study on the effect of Reynolds number on aerodynamic performance of high-speed train with and without yaw angle. *Journal of Wind Engineering & Industrial Aerodynamics* 157:36-46, DOI: 10.1016/j.jweia.2016.08.007

Pereira I, André JM CS (2013) A semi-analytical model of the 3D boundary layer over the streamlined nose of a train. *Journal of Wind Engineering & Industrial Aerodynamics* 119:78-88, DOI: 10.1016/j.jweia.2013.05.014

Schober M, Weise M, Orellano A, Deeg P, Wetzel W (2010) Wind tunnel investigation of an ICE 3 end car on three standard ground scenarios.

Journal of Wind Engineering & Industrial Aerodynamics 98:345-352, DOI: 10.1016/j.jweia.2009.12.004

Sterling M, Quinn AD, Hargreaves DM, Cheli F, Sabbioni E, Tomasini G, Delaunay D, Baker CJ, Morvan H (2010) A comparison of different methods to evaluate the wind induced forces on a high sided lorry. *Journal of Wind Engineering & Industrial Aerodynamics* 98:10-20, DOI: 10.1016/j.jweia.2009.08.008

Sun ZX, Guo DL, Yao Y (2013) Numerical study on ground effect of high-speed trains. *Journal of Chinese Computation Physics* 30(1):61-69 (in Chinese)

Xiang HY, Li YL, Chen SR, Li CJ (2017) A wind tunnel test method on aerodynamic characteristics of movingvehicles under crosswinds. *Journal of Wind Engineering & Industrial Aerodynamics* 163:15-23, DOI: 10.1016/j.jweia.2017.01.013

Xiao JP, Huang ZX, Chen L (2013) Review of aerodynamic investigation for high speed train. *Journal of Mechanics in Engineering* 35(2):1-12 (in Chinese)

Yang QS, Song JH, Yang GW (2016) A moving model rig with a scale ratio of 1/8 for high speed train aerodynamics. *Journal of Wind Engineering & Industrial Aerodynamics* 152:50-58, DOI: 10.1016/j.jweia.2016.03.002

Zhang L, Yang MZ, Liang XF (2018) Experimental study on the effect of wind angles on pressure distribution of train streamlined zone and train aerodynamic forces. *Journal of Wind Engineering & Industrial Aerodynamics* 174:330-348, DOI: 10.1016/j.jweia.2018.01.024